Monthly Notices
of the
ROYAL ASTRONOMICAL SOCIETY

MNRAS **450,** 4150–4160 (2015) doi:10.1093/mnras/stv840

Tracing the Galactic spiral structure with embedded clusters

D. Camargo,[1,2]★ C. Bonatto[1] and E. Bica[1]

[1]*Departamento de Astronomia, Universidade Federal do Rio Grande do Sul, Av. Bento Gonçalves 9500, Porto Alegre 91501-970, RS, Brazil*
[2]*Colégio Militar de Porto Alegre, Ministério da Defesa – Exército Brasileiro, Av. José Bonifácio 363, Porto Alegre 90040-130, RS, Brazil*

Accepted 2015 April 13. Received 2015 April 1; in original form 2015 January 16

ABSTRACT

In this work, we investigate the properties of 18 embedded clusters (ECs). The sample includes 11 previously known clusters and we report the discovery of seven ECs on *WISE* images, thus complementing our recent list of 437 new clusters. The main goal is to use such clusters to shed new light on the Galactic structure by tracing the spiral arms with cluster distances. Our results favour a four-armed spiral pattern tracing three arms, Sagitarius–Carina, Perseus, and the Outer arm. The Sagitarius–Carina spiral arm is probed in the borderline of the third and fourth quadrants at a distance from the Galactic Centre of $d_1 \sim 6.4$ kpc adopting $R_\odot = 7.2$ kpc, or $d_2 \sim 7.2$ kpc for $R_\odot = 8.0$ kpc. Most ECs in our sample are located in the Perseus arm that is traced in the second and third quadrants and appear to be at Galactocentric distances in the range $d_1 = 9$–10.5 kpc or $d_2 = 9.8$–11.3 kpc. Dolidze 25, Bochum 2, and Camargo 445 are located in the Outer arm that extends along the second and third Galactic quadrants with a distance from the Galactic Centre in the range of $d_1 = 12.5$–14.5 kpc or $d_2 = 13.5$–15.5 kpc. We find further evidence that in the Galaxy ECs are predominantly located within the thin disc and along spiral arms. They are excellent tools for tracing these Galactic features and therefore new searches for ECs can contribute to a better understanding of the Galactic structure. We also report an EC aggregate located in key italicthe Perseus arm.

Key words: astronomical data bases: miscellaneous – catalogues – Galaxy: disc – open clusters and associations: general – Galaxy: structure.

1 INTRODUCTION

Despite the effort that has been made to improve our understanding of the Galactic structure, questions about the spiral arm nature (Baba et al. 2009; Sellwood 2011; Grand, Kawata & Cropper 2012; Martínez-García & González-López lira 2013; Roca-Fàbrega et al. 2013; Sellwood & Carlberg 2014), structure (Georgelin & Georgelin 1976; Russeil 2003; Levine, Blitz & Heiles 2006; Majaess, Turner & Lane 2009; Hou & Han 2014), and dynamics (Fujii et al. 2011; Binney et al. 2014) remain open. There is no consensus on the number, pitch angle, and shape of Galactic spiral arms (Vallée 2005, 2014a,b; Hou, Han & Shi 2009; Lépine et al. 2011; Francis & Anderson 2012; Siebert et al. 2012; Bobylev & Bajkova 2014; Griv et al. 2014; Pettitt et al. 2014). The Sun's location within the dust obscured Galactic disc is a complicating factor to observe the Galactic structure.

It is widely accepted that spiral arms are the preferred sites of star formation and, as most stars form within embedded cluster (EC) the arms are sites of cluster formation. Star formation may occur after the collapse and fragmentation of giant molecular clouds (GMCs) that occur within spiral arms transforming dense gas clumps into ECs. Based on the absence of massive ^{13}CO bright molecular clouds in the interarm space, Roman-Duval et al. (2009) argue that molecular clouds must form in spiral arms and be short-lived (less than 10 Myr). Then, the spiral arms may be traced by young star clusters, especially ECs that have not had enough time to move far from their birth places. In addition, EC parameters are derived with good accuracy. In this sense, ECs with derived parameters can be used to distinguish between the various theoretical models for spiral arm structure (Dobbs & Pringle 2010; Sellwood 2010). Besides constraining the spiral arm distribution with direct distances, ECs can also contribute to kinematic modelling of the spiral structure (Georgelin & Georgelin 1976; Russeil 2003).

We have contributed significantly to increase the number of ECs with derived parameters (Camargo, Bonatto & Bica 2009, 2010, 2011, 2012; Camargo, Bica & Bonatto 2013, 2015a). Besides deriving parameters, in Camargo et al. (2015a) we discovered 437 ECs and stellar groups increasing the Galactic EC sample. Majaess (2013) has also made a significant contribution on young clusters (see also, Bica, Dutra & Barbuy 2003a; Bica et al. 2003b; Lada & Lada 2003; Mercer et al. 2005; Froebrich, Scholz & Raftery 2007; Borissova et al. 2011; Solin, Haikala & Ukkonen 2014).

The main goal of this work is deriving accurate cluster parameters to use as tools to provide new constraints to better understand the Galactic structure. We also present new ECs discovered by

★E-mail: denilso.camargo@ufrgs.br

Table 1. General data of the present star clusters.

Target	α(2000) (h m s)	δ(2000) (° arcmin arcsec)	ℓ (°)	b (°)	Comments
(1)	(2)	(3)	(4)	(5)	(6)
IRAS 0207+6047 Cl.	2:44:37	60:59:42	136.22	1.08	also known as BDB 116 and Majaess 30
SAI 23	2:54:10	60:39:02	137.42	1.28	Glushkova et al. (2010)
Camargo 440	3:59:58	51:33:23	150.05	−1.11	This work
BDS 61	4:03:17	51:19:35	150.59	−0.94	Bica et al. (2003b)
Camargo 441	4:03:18	51:29:37	150.48	−0.81	This work
Camargo 442	4:04:14	51:22:56	150.66	−0.80	This work
FSR 665	4:04:59	51:31:35	150.65	−0.62	Froebrich et al. (2007)
FSR 666	4:05:51	51:28:35	150.79	−0.56	Froebrich et al. (2007)
Camargo 443	4:07:08	51:11:14	151.13	−0.64	This work
Camargo 444	4:07:49	51:15:23	151.16	−0.52	This work
Camargo 445	4:08:12	50:31:29	151.70	−1.02	This work (in Majaess 45)
BDS 65	4:11:10	51:09:58	151.61	−0.23	Bica et al. (2003b)
Camargo 446	6:10:27	16:43:14	193.43	−1.17	This work
Camargo 63	6:12:01	13:39:36	196.30	−2.31	Camargo et al. (2015a)
Majaess 78	6:13:39	15:58:07	194.46	−0.87	Majaess (2013)
Dolidze 25	6:45:02	00:13:21	212.00	−1.33	Moffat & Vogt (1975)
Bochum 2	6:48:50	00:22:44	212.29	−0.40	Turbide & Moffat (1993)
NGC 2367	7:20:07	−21:52:57	235.60	−3.83	Vogt & Moffat (1972)

Notes. Cols. 2–3: central coordinates. Cols. 4–5: corresponding Galactic coordinates. Col. 6: comments.

Figure 1. *WISE* RGB image of the Perseus 1 aggregate: FSR 665, FSR 666, Camargo 441, Camargo 442, Camargo 443, Camargo 444, BDS 61, BDS 62, and BDS 63.

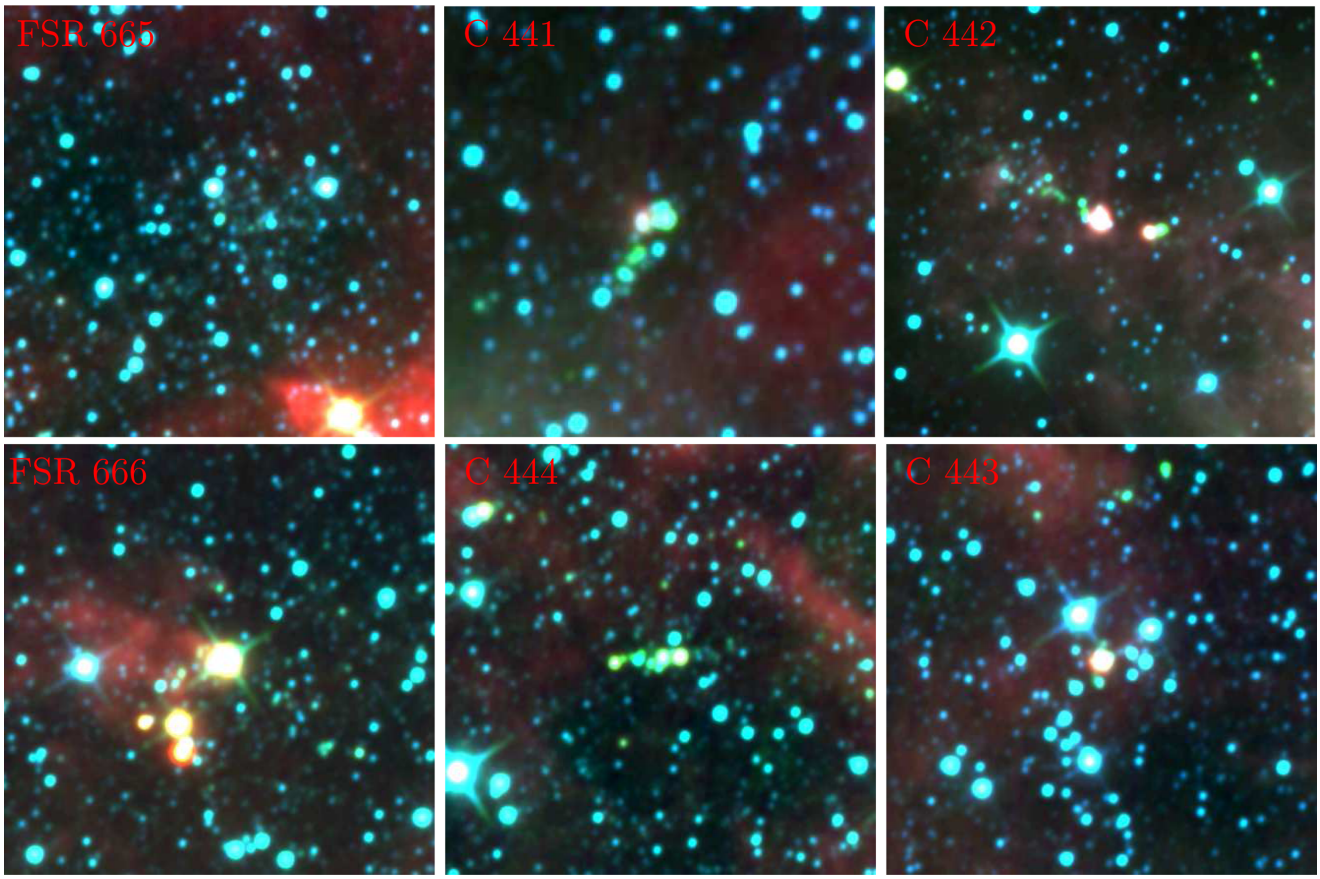

Figure 2. *WISE* RGB images centred on FSR 665 (10 arcmin × 10 arcmin), Camargo 441 (7 arcmin × 7 arcmin), Camargo 442 (12 arcmin × 12 arcmin), FSR 666 (10 arcmin × 10 arcmin), Camargo 444 (10 arcmin × 10 arcmin), and Camargo 443 (10 arcmin × 10 arcmin).

ourselves as a follow up of our recent catalogue (Camargo et al. 2015a; Camargo, Bica & Bonatto 2015b). The searches for new clusters were made by eye on *WISE* images.

The paper is organized as follows. In Section 2, we describe the methods and tools employed in the cluster analyses. In Section 3, we present the results of the cluster analysis, and derive parameters (age, reddening, distance, core, and cluster radii). In Section 4, we discuss the results. Finally, in Section 5 we provide the concluding remarks.

2 METHODS OF ANALYSIS

Cluster fundamental parameters are derived using Two Micron All Sky Survey (2MASS)[1] photometry (Skrutskie et al. 2006) in the J, H, and K_s bands, extracted in circular concentric regions centred on the coordinates given in Table 1 and fitted with PARSEC isochrones (Bressan et al. 2012). The fits are made by eye, taking the combined main sequence (MS) and pre-main sequence (PMS) stellar distributions as constraints, and allowing for variations due to photometric uncertainties and differential reddening.

The process relies on application of shifts in magnitude and colour in the isochrone set (MS + PMS) from the zero distance modulus and reddening until a satisfactory solution is reached. The best fits are superimposed on decontaminated colour-magnitude diagrams (CMDs) (Figs 3 to 9).

[1] The Two Micron All Sky Survey, available at www.ipac.caltech.edu/2mass/releases/allsky/.

To uncover the intrinsic CMD morphology, we apply a field-star decontamination procedure. The algorithm works on a statistical basis by measuring the relative number densities of probable cluster and field stars in 3D CMD cells that have axes along the J, $(J - H)$, and $(J - K_s)$ magnitude and colours (Bonatto & Bica 2007b; Bica, Bonatto & Camargo 2008; Bonatto & Bica 2008, 2010). Then, the algorithm subtracts the expected number of field stars from each cell. It has been used in several works (e.g. Bonatto & Bica 2009, 2011a; Camargo et al. 2009, 2010, 2011, 2012, 2013; Bica & Bonatto 2011, and references therein).

The cluster structure is analysed by means of the stellar radial density profile (RDP) built with stars selected after applying the respective colour–magnitude (CM) filter to the observed photometry. The CM filter excludes stars with different colours of those within the probable cluster sequences and enhances the RDP contrast relative to the background (e.g. Bonatto & Bica 2007a, and references therein). Structural parameters are derived by fitting King-like profiles to the clusters RDPs (King 1962). This procedure was applied in previous works (e.g. Bonatto & Bica 2010, 2011b; Bica & Bonatto 2011; Lima et al. 2014, and references therein).

3 RESULTS

NASA's *WISE* telescope observed the whole sky in the bands $W1$ (3.4 μm), $W2$(4.6 μm), $W3$(12 μm), and $W4$ (22 μm). $W1$ and $W2$ are particularly sensitive to the EC stellar content, while $W3$ and $W4$ show mostly dust emission.

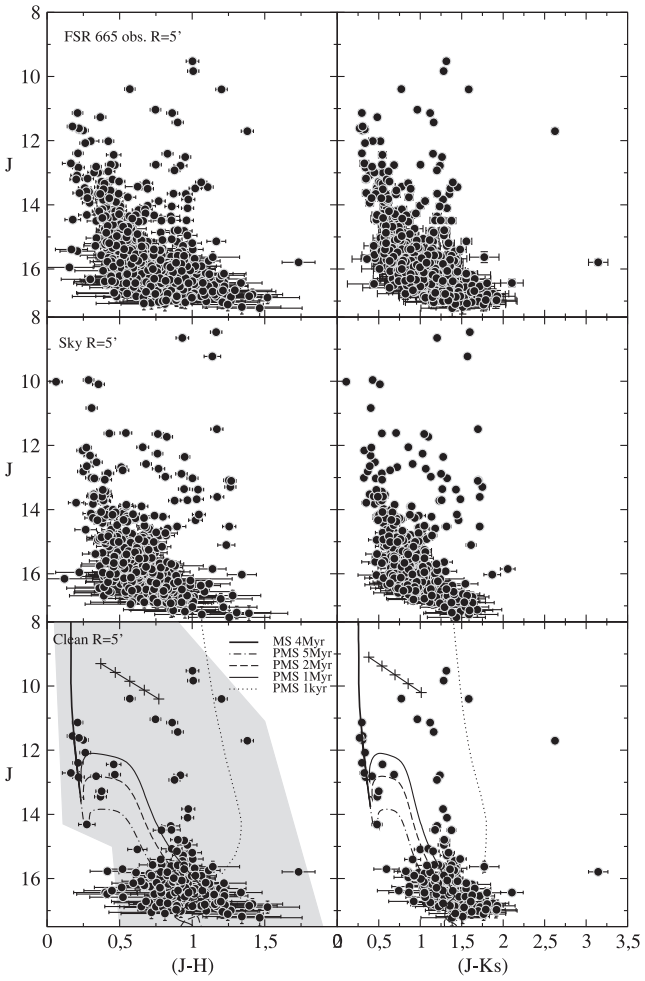

Figure 3. 2MASS $J \times (J - H)$ and $J \times (J - K_s)$ CMDs for FSR 665. Top panels: observed CMDs. Middle: equal area comparison field. Bottom: field-star decontaminated CMDs. The decontaminated CMD of FSR 665 was fitted with PARSEC isochrones for both MS and PMS stars. The CM filter used to isolate cluster stars is shown as a shaded region. We also show the reddening vector for $A_V = 0$–5.

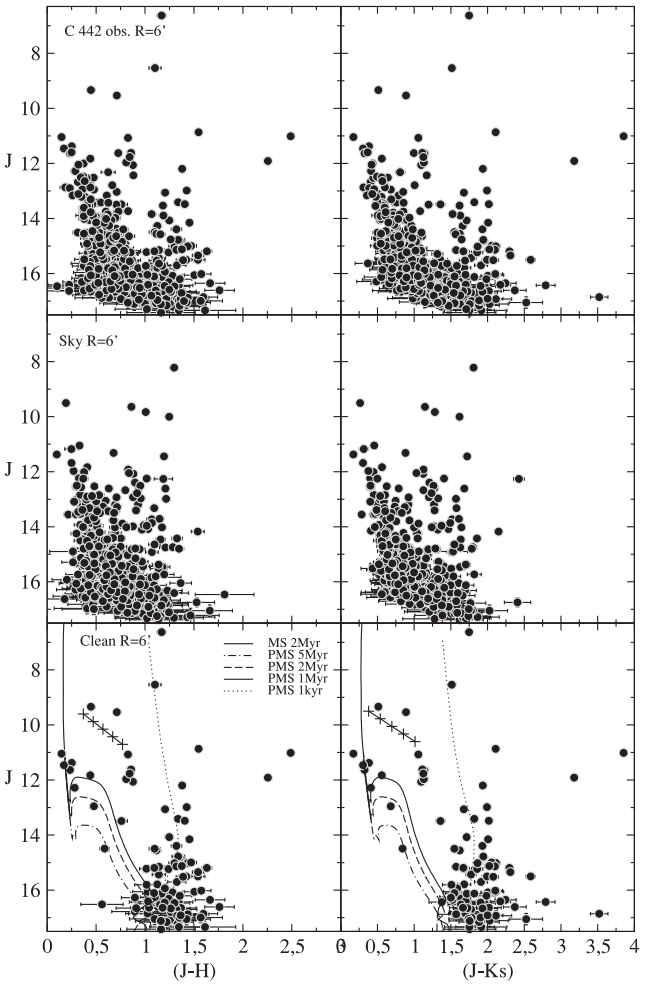

Figure 4. Same as Fig. 3 for Camargo 442.

Figs 1 and 2 show *WISE* composite images for BDS 61, BDS 65, C 441, C 442, C 443, C 444, FSR 665, and FSR 666. Figs 3–9 show CMDs for all objects in Table 1. RDPs are presented in Figs 10 and 11. Fundamental parameters are shown in Table 2 and the structure for clusters that can be described by a King law are shown in Table 3.

3.1 Previously known star clusters

IRAS 0207+6047 Cluster (BDB 116): we derived an age of 2 ± 1 Myr for a distance of $d_\odot = 2.8 \pm 0.4$ kpc (Fig. 9). The structure of this object points to a cluster, but cannot be fitted by a King-like function (Fig. 11).

SAI 23: fitting isochrones to cluster decontaminated CMD (Fig. 6), we derive an age of ∼4 Myr for a distance of $d_\odot = 2.8 \pm 0.4$ kpc. From the RDP (Fig. 10), we found $R_c = 0.85 \pm 0.1$ pc, $\sigma_{0K} = 25.2 \pm 3.6$ stars pc^{-2}, and a cluster RDP radius of 10.01 ± 2.3 pc.

BDS 61: is an EC located in the Perseus arm presenting an O-type star in the central region ($R < 1$ arcmin), as shown by the decontaminated CMD (Fig. 8). We derive an age of ∼1 Myr for a $d_\odot = 2.7 \pm 0.3$ kpc. Despite a dip in the inner RDP region, the structure of BDS 61 is consistent with an EC in the early evolutionary phase (Fig. 11).

FSR 665: located close to the Perseus arm, this object is a prominent EC with a relatively well-developed MS and a populous PMS (Fig. 3). The best fit of PARSEC isochrones (MS + PMS) suggest an age of ∼4 Myr and a $d_\odot = 2.9 \pm 0.3$ kpc. The presence of other ECs creates a bump in the FSR 665 RDP (Fig. 10).

FSR 666: *WISE* images (Figs 1 and 2) of FSR 666 point to ongoing star formation. The decontaminated CMD and the respective MS and PMS isochrone fits provide an age of ∼1 Myr for a $d_\odot = 2.8 \pm 0.7$ kpc, which put this EC in the Perseus arm. The RDP of FSR 666 is irregular and cannot be fitted by a King-like profile (Fig. 11), but suggests a cluster. Note that young clusters lack the span of time to be an isothermal sphere.

BDS 65: located in the Perseus arm at a $d_\odot = 2.5 \pm 0.4$ kpc. The object is a prominent EC, as indicated by CMDs (Fig. 8) and RDP (Fig. 11). The decontaminated CMD of BDS 65 shows a very reddened O star within the central region ($R < 1$ arcmin) and suggests an age of ∼1 Myr. The RDP presents a high contrast with respect to the background, but King profile cannot be fitted.

Camargo 63: recently discovered by Camargo et al. (2015a) this EC is confirmed as a cluster in this work. The decontaminated CMD of C 63 fitted by PARSEC isochrones (Fig. 6) suggests an age of

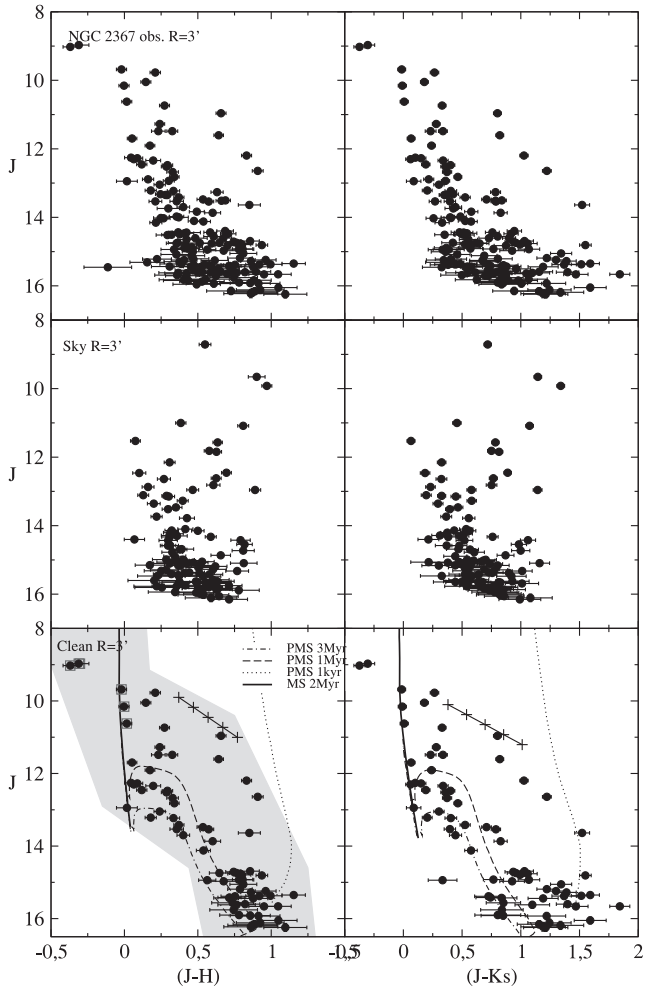

Figure 5. Same as Fig. 3 for NGC 2367. The squares on the decontaminated CMDs indicate B stars.

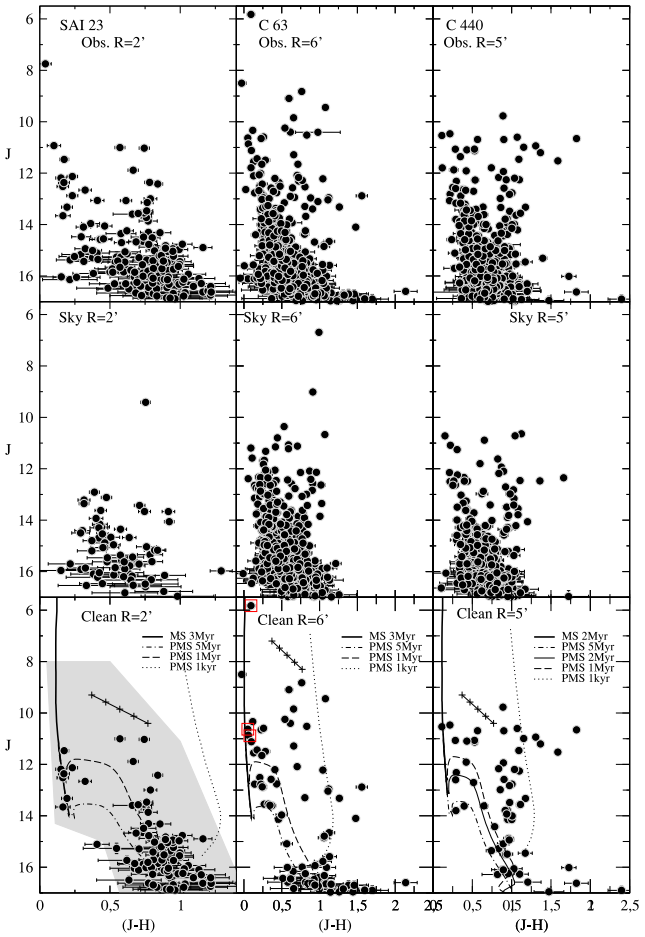

Figure 6. 2MASS CMDs of the ECs SAI 23, Camargo 63, and Camargo 440. Top panels: observed CMDs $J \times (J-H)$. Middle panels: equal area comparison field. Bottom panels: field-star decontaminated CMDs fitted with MS and PMS PARSEC isochrones. The CM filters used to isolate cluster stars are shown as shaded regions (only for clusters with RDP following a King-like profile). The squares on the decontaminated CMDs indicate B stars. We also present the reddening vector for $A_V = 0$ to 5.

∼3 Myr and present three B stars in the central region. We found a distance from the Sun of 3.3 ± 0.5 kpc, close to the Perseus arm. The RDP of C 63 is irregular (Fig. 11), certainly owing to absorption effects in the 2MASS bands.

Majaess 78: our analyses (Fig. 9) suggest that this EC lies in the Perseus arm at a distance of 3.2 ± 0.5 kpc and presents an age of ∼3 Myr. Fig. 11 shows the irregular RDP for Majaess 78.

Dol 25: Moffat & Vogt (1975) derived a distance from the Sun of 5.25 kpc and Lennon et al. (1990) a $d_\odot = 5.5 \pm 0.5$ kpc. We argue that Dol 25 is related to Sh2-284 and lies at $d_\odot = 5.5 \pm 0.8$ kpc. We obtained an age of ∼2 Myr for Dol 25. Five B-type stars are found in the central region of the cluster. The inner region of the cluster ($R < 1$ arcmin) contains four of the massive B stars shown in the decontaminated CMD (Fig. 8). The RDP fitted by a King-like profile (Fig. 10) gives $R_c = 0.31 \pm 0.06$ pc, $\sigma_{0K} = 21.42 \pm 5.98$ stars pc^{-2}, and $R_{\rm RDP} = 8.05 \pm 3.22$ pc. The RDP irregularities at large radii are probably caused by stellar overdensities in the Dol 25 neighbourhood, probably related to sequential star formation.

Bochum 2: Stephenson & Sanduleak (1971) found a distance from the Sun of 5.5 kpc for Bo 2. subsequently, Moffat, Jackson & Fitzgerald (1979) estimated a distance of 4.8 kpc. Munari & Carraro (1995) estimated an age of 7 Myr for a distance from Sun of ∼6 kpc. Our analyses of the decontaminated CMD of Bo 2 (Fig. 8) suggest an age of ∼5 Myr and a $d_\odot = 7.9 \pm 1.1$ kpc. This EC lies in the Outer arm. The O stars shown in the decontaminated CMD are members of binary systems and are located in the inner cluster radius ($R < 1$ arcmin). The RDP of Bo 2 provides $R_c = 0.57 \pm 0.16$ pc, $\sigma_{0K} = 7 \pm 3$ stars pc^{-2} for a cluster radius of 9.2 ± 2.3 pc.

NGC 2367: Carraro et al. (2005) derived an age of 5 Myr and a distance from the Sun of 1.4 kpc for NGC 2367 while Santos-Silva & Gregorio-Hetem (2012) derived an age of 3 Myr and $d_\odot \sim 2.2$ kpc. We estimated an age of 2 ± 1 Myr and $d_\odot = 3.4 \pm 0.7$ kpc for NGC 2367. It presents five B stars in the central region, two of them with J excess (Fig. 5). The cluster shows a smooth RDP (Fig. 10) with $\sigma_{0K} = 24.64 \pm 13.64^{\star}$ pc^{-2} and $R_{\rm RDP} = 4.75 \pm 0.47$ pc. Both, CMDs and RDP suggest that this EC will evolve to become a classical OC.

3.2 Present work discoveries

We discovered in this work seven new ECs. The newly found star clusters complement our previous catalogue (Camargo et al. 2015a,b).

Camargo 440: this new EC is located in the Perseus arm at a $d_\odot = 2.6 \pm 0.4$ kpc. Based on the cluster CMD (Fig. 6), we

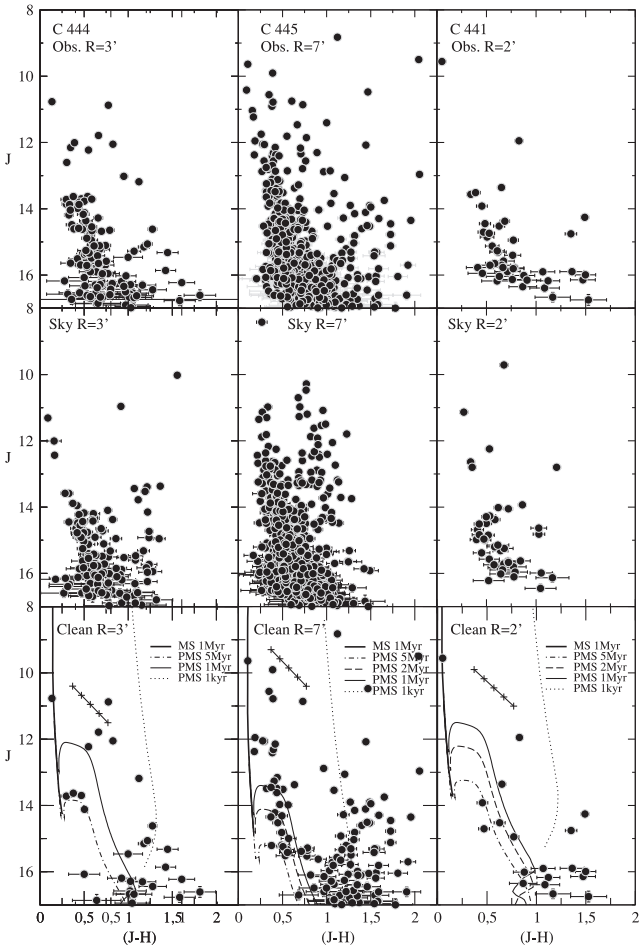

Figure 7. Same as Fig. 6 for Camargo 444, Camargo 445, and Camargo 441.

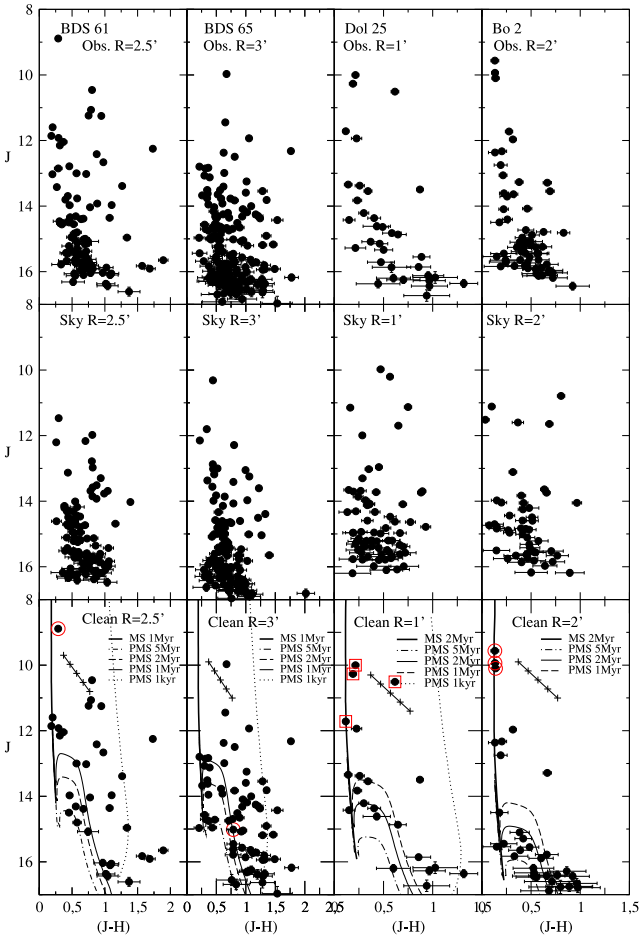

Figure 8. Same as Fig. 6 for BDS 61, BDS 65, Dolidze 25, and Bochum 2. The circles on the decontaminated CMDs indicate O stars and the squares B stars.

estimated an age of ∼1 Myr. The overdensity in the outermost RDP of C 440 is due to King 7 (Fig. 11).

Camargo 441: this EC present an age of 1 Myr and is located at a $d_{\odot} = 2.5 \pm 0.5$ kpc in the Perseus arm. Both the decontaminated CMD (Fig. 8) and RDP (Fig. 11) suggest a small poor cluster.

Camargo 442: this EC lies in the Perseus arm at a $d_{\odot} = 2.7 \pm 0.4$ kpc. The best isochrone fit (Fig. 4) provides an age of ∼1 Myr. The irregular RDP (Fig. 11) does not follow a cluster-like profile.

Camargo 443: this previously unknown EC lies in the Perseus arm at a distance of $d_{\odot} = 3.1 \pm 0.7$ kpc. C 443 is ∼3 Myr old and presents a well-defined MS and PMS with very reddened stars (Fig. 9). Its RDP suggests a cluster, but does not follow a King-like profile (Fig. 11), which is expected for young clusters (Camargo et al. 2015a).

Camargo 444: lies at a distance of $d_{\odot} = 3.0 \pm 0.7$ kpc in the Perseus arm. The analysis of the images (Figs 1 and 2) and decontaminated CMD (Fig. 7) suggests ages of ∼1–2 Myr. The RDP (Fig. 10) points to cluster, but cannot be fitted by King-like profile.

Camargo 445: we derive via the decontaminated CMD (Fig. 7) analysis an age of ∼1 Myr and a $d_{\odot} = 6.3 \pm 0.9$ kpc, which sets this EC in the Outer arm. The RDP of C 445 is irregular and cannot be fitted by a King-like profile (Fig. 11).

Camargo 446: this object is an EC with an age of ∼1 Myr and is located in the Perseus arm at a distance of $d_{\odot} = 2.9 \pm 0.4$ kpc (Fig. 9). The RDP does not follow a King law (Fig. 11).

4 DISCUSSION

The present analysis places the ECs BDS 61, C 441, C 442, C 443, C 444, FSR 665, and FSR 666 in the same region in the Perseus arm. Fig. 1 presents this star cluster aggregate (hereafter Perseus 1 cluster aggregate) formed by ECs with similar ages. Such groups were predicted or observed by Efremov (1995), de la Fuente Marcos & de la Fuente Marcos (2008, 2009a, 2010), Guillout et al. (1998), Fellhauer & Kroupa (2005), Camargo et al. (2011, 2012, 2013, 2015a) and Feigelson et al. (2011). Several large dust emission bubbles in *WISE* images connect these clusters, suggesting second generation effects (Camargo et al. 2015a). This leaves open the possibility that an entire GMC may fragment almost simultaneously forming a large EC aggregate. The spiral arms may play an important role in the erosion of a GMC triggering massive star formation in the whole cloud. Camargo et al. (2012) pointed out the star formation within cluster groups. They suggest that an irregular GMC (or complex) may form massive stars simultaneously and their winds and/or supernova explosions may produce a second generation of massive stars propagating the star formation and producing star clusters with similar age. The ECs formation is quite rapid and probably range from 0.5–5 Myr (Lada & Lada 2003; Allen et al. 2007; Tamburro et al. 2009; Santos-Silva & Gregorio-Hetem 2012; Camargo et al. 2013). According to Camargo et al. (2013), the deep embedded phase for most Galactic ECs ends before 3 Myr (Ballesteros-Paredes & Hartmann 2007; de la Fuente

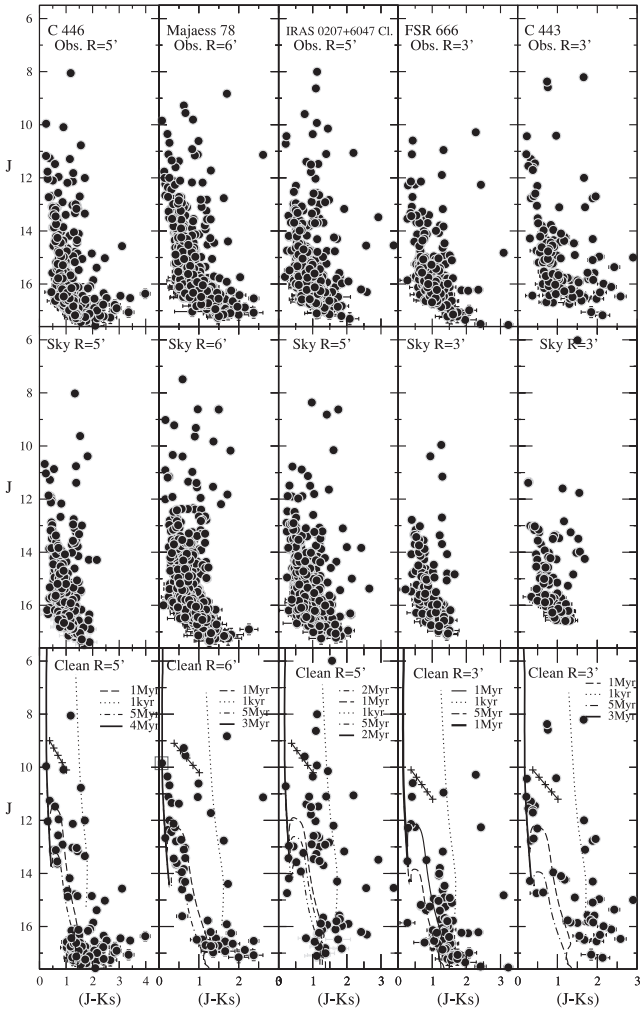

Figure 9. 2MASS CMDs for the clusters Camargo 446, Majaess 78, IRAS 0207 + 6047 Cl., FSR 666, and Camargo 443. Top panels: observed CMDs $J \times (J - K_s)$. Middle panels: equal area comparison field. Bottom panels: field-star decontaminated CMDs fitted with MS and PMS PARSEC isochrones. We also present the reddening vector for $A_V = 0$–5.

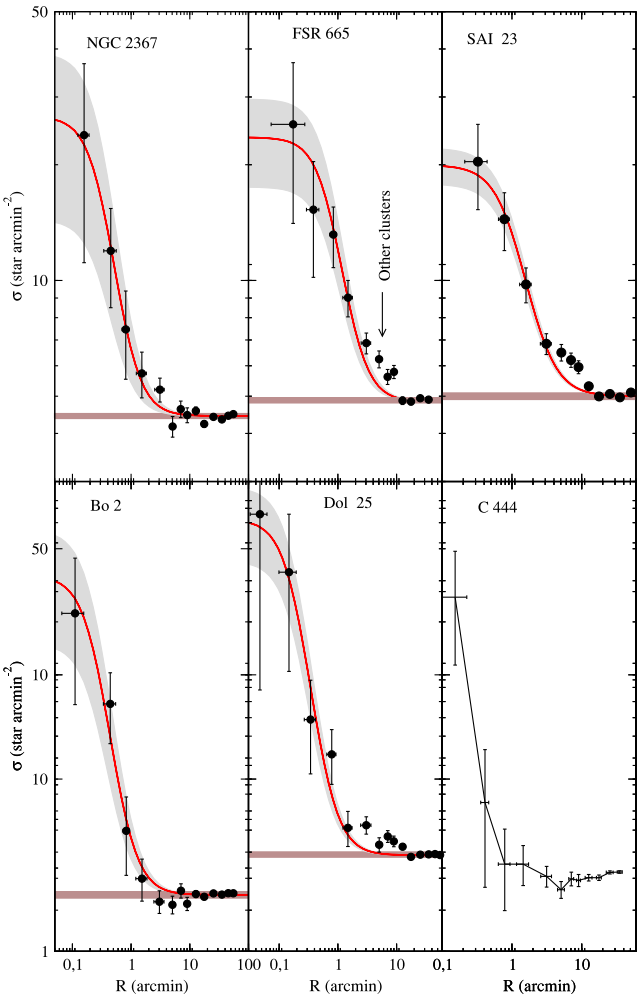

Figure 10. RDPs for the ECs NGC 2367, FSR 665, SAI 23, Bochum 2, Dolidze 25, and Camargo 444. Brown horizontal shaded region: stellar background level measured in the comparison field. Grey regions: 1σ King fit uncertainty.

Marcos & de la Fuente Marcos 2009b). Bally (2008) argue that OB associations consist of sub-groups, clusters, and sub-clusters with no preferred scale (Jose et al. 2013). The GMC W51 with an EC aggregate distributed inside ≈100 pc may be an example of this scenario (Kumar, Kamath & Davis 2004). Several H II regions in Anderson et al. (2014) are within complexes. Several EC candidates from Solin et al. (2014) have neighbours. The present Perseus 1 aggregate of ECs is similar to the Auriga 1 aggregate, recently found by Camargo et al. (2012).

The large-scale cluster formation within the structure shown in Fig. 1 may be a consequence of the Perseus arm gas compression, but the small-scale cluster distribution suggest sequential formation.

Dol 25 is located in the centre of a large bubble and apparently is triggering a sequential star formation event, forming a second EC generation (Lee, Murray & Rahman 2012; Camargo, Bica & Bonatto 2015a). In this sense, EC aggregates appear to be formed in sequential events.

BDS 61, BDS 65, Dol 25, and Bochum 2 present massive stars located within their central region ($R < 1$ arcmin).

4.1 Galactic distribution

Fig. 12 updates the previous version in fig. 14 in Camargo et al. (2013). Black circles are clusters in this work and brown circles ECs from our previous studies (Camargo et al. 2010, 2011, 2012, 2013, 2015a).

Following Camargo et al. (2013), most ECs are found in the thin disc within 250 pc from the Galactic mean plane (Vallenari, Bertelli & Schmidtobreick 2000; Siebert, Bienaymé & Soubiran 2003) as shown in panels (b), (c), and (d). The Z_{GC} distribution of the present cluster sample (Table 2) is consistent with Buckner & Froebrich (2014) result for the Galactic cluster scaleheight. However, some ECs are found at large distances from the Galactic plane (Fig. 12), mainly in the spiral arms (Camargo et al. 2013).

The Sagittarius–Carina spiral arm is well traced by the subsample of clusters with derived parameters in our recent discovered ECs (Camargo et al. 2015a). This spiral arm is presently probed near the borderline of the third and fourth quadrants at a distance from the Galactic Centre of $d_1 \sim 6.4$ kpc or $d_2 \sim 7.2$ kpc.

Most ECs in the present sample are distributed in the second and third quadrants along the Perseus arm. In this region the Perseus arm is located at Galactocentric distances in the range of 9 kpc in the second quadrant to 10.5 kpc in the third quadrant for a distance

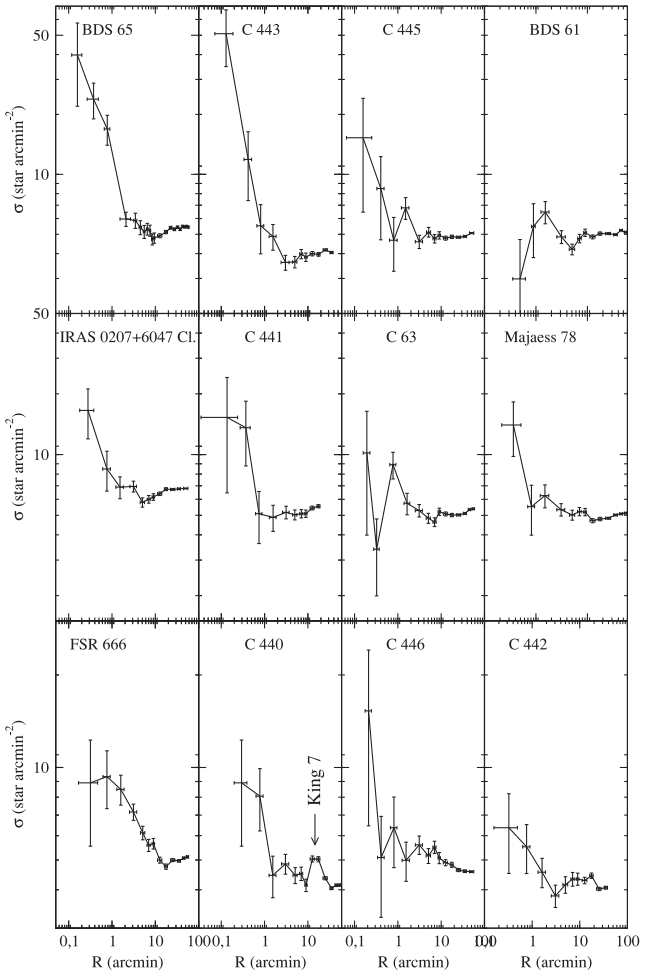

Figure 11. RDPs for the confirmed clusters BDS 65, Camargo 443, Camargo 445, BDS 61, IRAS 0207+6047 Cl., Camargo 441, Camargo 63, Majaess 78, FSR 666, Camargo 440, Camargo 446, and Camargo 442.

of the Sun to the Galactic Centre of 7.2 kpc or in the range of 9.8–11.3 kpc for $R_\odot = 8.0$ kpc.

The presence of molecular clouds beyond the Perseus arm is known since a few decades (Digel, de Geus & Thaddeus 1994; Heyer & Terebey 1998). Kaltcheva & Hilditch (2000) proposed the existence of a spiral arm in the Outer Galaxy, the Outer arm. Since then, several works have been developed, but the Outer arm is still not fully traced (Russeil 2003; Pandey, Sharma & Ogura 2006; Honma et al. 2007; Russeil, Adami & Georgelin 2007; Hachisuka et al. 2009, and references therein). In Camargo et al. (2013), based on the distribution of ECs, we confirmed that the Outer arm extends along the second and third Galactic quadrants with Galactocentric distances in the range of 12.5–14.5 kpc for $R_\odot = 7.2$ kpc or 13.5–15.5 kpc for $R_\odot = 8.0$ kpc. The distance from the Sun and Galactocentric radii derived for the Outer arm in this work agrees with Hachisuka et al. (2009) results. There is a large discrepancy between the stellar Outer arm and the gaseous Outer arm with distance larger than 20 kpc, but it appears to be a common feature for large spiral galaxies (McClure-Griffiths et al. 2004).

5 CONCLUDING REMARKS

In this work, we investigate the properties of 18 ECs. Besides 11 previously known clusters we discovered seven ECs, some of them

Table 2. Derived fundamental parameters for ECs in the present study.

Cluster	$E(J-H)$ (mag)	Age (Myr)	$d_\odot$ (kpc)	R_{GC} (kpc)	x_{GC} (kpc)	y_{GC} (kpc)	z_{GC} (pc)	R_{GC} (kpc)	x_{GC} (kpc)	y_{GC} (kpc)	z_{GC} (pc)
(1)	(2)	(3)	(4)	(5)	(6)	(7)	(8)	(9)	(10)	(11)	(12)
IRAS 0207+6047 Cl.	0.28 ± 0.02	2 ± 1	2.8 ± 0.4	9.4 ± 0.3	−9.25 ± 0.28	1.94 ± 0.27	52.8 ± 7.4	10.51 ± 0.28	−10.33 ± 0.28	1.94 ± 0.27	52.89 ± 7.42
SAI 23	0.28 ± 0.02	4 ± 1	2.7 ± 0.4	9.4 ± 0.3	−9.19 ± 0.28	1.81 ± 0.25	59.8 ± 8.4	10.43 ± 0.28	−10.27 ± 0.28	1.81 ± 0.25	59.86 ± 8.40
Camargo 440	0.27 ± 0.02	1 ± 0.5	2.6 ± 0.4	9.5 ± 0.3	−9.46 ± 0.31	1.29 ± 0.18	−50.2 ± 7.0	10.62 ± 0.31	−10.54 ± 0.31	1.29 ± 0.18	−50.20 ± 7.04
BDS 61	0.23 ± 0.03	2 ± 1	2.7 ± 0.3	9.7 ± 0.3	−9.59 ± 0.335	1.34 ± 0.18	−44.7 ± 6.2	10.76 ± 0.33	−10.68 ± 0.33	1.32 ± 0.18	−21.27 ± 2.95
Camargo 441	0.21 ± 0.03	1 ± 0.5	2.5 ± 0.5	9.5 ± 0.4	−9.44 ± 0.42	1.26 ± 0.24	−36.0 ± 6.8	10.59 ± 0.41	−10.52 ± 0.42	1.26 ± 0.24	−36.01 ± 6.76
Camargo 442	0.32 ± 0.02	1 ± 1	2.7 ± 0.4	9.6 ± 0.3	−9.55 ± 0.34	1.31 ± 0.19	−37.3 ± 5.5	10.71 ± 0.34	−10.63 ± 0.34	1.31 ± 0.19	−37.27 ± 5.47
FSR 665	0.32 ± 0.03	4 ± 1.5	2.9 ± 0.3	9.9 ± 0.2	−9.77 ± 0.2	1.43 ± 0.14	−31.7 ± 3.0	10.95 ± 0.24	−10.85 ± 0.24	1.43 ± 0.14	−31.67 ± 3.02
FSR 666	0.27 ± 0.03	1 ± 1	2.8 ± 0.7	9.8 ± 0.6	−9.70 ± 0.58	1.39 ± 0.32	−27.9 ± 6.5	10.87 ± 0.57	−10.78 ± 0.58	1.39 ± 0.32	−27.77 ± 6.47
Camargo 443	0.30 ± 0.02	3 ± 1	3.1 ± 0.7	10.1 ± 0.6	−9.97 ± 0.65	1.52 ± 0.36	−35.1 ± 8.3	11.16 ± 0.64	−11.05 ± 0.65	1.52 ± 0.36	−35.10 ± 8.26
Camargo 444	0.29 ± 0.03	2 ± 1	3.0 ± 0.7	10.0 ± 0.6	−9.88 ± 0.63	1.47 ± 0.34	−27.6 ± 6.5	10.93 ± 0.35	−10.84 ± 0.36	1.40 ± 0.20	−26.34 ± 3.69
Camargo 445	0.26 ± 0.02	1 ± 0.5	6.3 ± 0.9	13.1 ± 0.7	−12.76 ± 0.78	2.98 ± 0.42	−112.1 ± 15.7	14.16 ± 0.76	−13.84 ± 0.78	2.98 ± 0.42	−112.05 ± 15.71
BDS 65	0.22 ± 0.03	1 ± 1	2.5 ± 0.4	9.5 ± 0.3	−9.43 ± 0.33	1.20 ± 0.18	−10.1 ± 6.2	10.58 ± 1.02	−10.51 ± 1.02	1.20 ± 0.55	−10.15 ± 4.68
Camargo 446	0.14 ± 0.01	1 ± 0.5	2.9 ± 0.4	10.1 ± 0.4	−10.05 ± 0.39	−0.68 ± 0.09	−59.4 ± 8.2	11.15 ± 0.39	−11.13 ± 0.39	−0.68 ± 0.09	−59.44 ± 8.24
Camargo 63	0.14 ± 0.02	3 ± 1	3.3 ± 0.5	10.5 ± 0.4	−10.43 ± 0.45	−0.94 ± 0.13	−131.2 ± 18.4	11.54 ± 0.45	−11.51 ± 0.45	−0.94 ± 0.13	−131.22 ± 18.40
Majaess 78	0.22 ± 0.02	5 ± 3	3.2 ± 0.5	10.3 ± 0.5	−10.29 ± 0.50	−0.79 ± 0.13	−47.5 ± 7.7	11.39 ± 0.50	−11.37 ± 0.50	−0.79 ± 0.13	−47.54 ± 7.74
Dolidze 25	0.25 ± 0.01	2 ± 1	5.5 ± 0.8	12.3 ± 0.7	−11.93 ± 0.66	−2.94 ± 0.66	−128.9 ± 18.1	13.34 ± 0.65	−13.01 ± 0.66	−2.94 ± 0.41	−128.85 ± 18.07
Bochum 2	0.30 ± 0.01	5 ± 1	7.9 ± 1.1	14.5 ± 0.9	−13.89 ± 0.92	−4.22 ± 0.58	−55.1 ± 7.6	15.56 ± 0.90	−14.97 ± 0.92	−4.22 ± 0.58	−55.11 ± 7.64
NGC 2367	0.12 ± 0.01	2 ± 1	3.3 ± 0.7	9.5 ± 0.4	−9.06 ± 0.42	−2.69 ± 0.62	−218.6 ± 50.4	10.50 ± 0.44	−10.14 ± 0.42	−2.69 ± 0.62	−218.60 ± 50.35

Notes. Col. 2: $E(B-V)$ in the cluster's central region. Col. 3: age, from 2MASS photometry. Col. 4: distance from the Sun. Col. 5: R_{GC} calculated using $R_\odot = 7.2$ kpc for the distance of the Sun to the Galactic Centre (Bica et al. 2006). Cols. 6–8: Galactocentric components using $R_\odot = 7.2$ kpc. Col. 9: R_{GC} calculated using $R_\odot = 8.3$ kpc for the distance of the Sun to the Galactic Centre. Cols. 10–12: Galactocentric components using $R_\odot = 8.3$ kpc.

Table 3. Structural parameters for clusters in the current sample.

Cluster	(1 arcmin) (pc)	σ_{0K} (* pc^{-2})	$R_{\rm core}$ (pc)	$R_{\rm RDP}$ (pc)	σ_{0K} (* arcmin^{-2})	$R_{\rm core}$ (arcmin)	$R_{\rm RDP}$ (arcmin)
(1)	(2)	(3)	(4)	(5)	(6)	(7)	(8)
SAI 23	0.77	25.23 ± 3.63	0.85 ± 0.10	10.01 ± 2.31	14.96 ± 2.15	1.11 ± 0.13	13.0 ± 3.0
FSR 665	0.85	25.92 ± 8.4	0.67 ± 0.16	6.97 ± 2.55	18.73 ± 6.07	0.79 ± 0.19	8.2 ± 3.0
Dol 25	1.61	21.42 ± 5.98	0.31 ± 0.06	8.05 ± 3.22	55.52 ± 15.50	0.19 ± 0.04	5.0 ± 2.0
Bo 2	2.29	7.03 ± 2.97	0.57 ± 0.16	9.16 ± 2.30	36.85 ± 15.59	0.25 ± 0.07	4.0 ± 1.0
NGC 2367	0.95	24.64 ± 13.64	0.31 ± 0.12	4.75 ± 0.47	22.24 ± 12.31	0.33 ± 0.13	5.0 ± 0.5

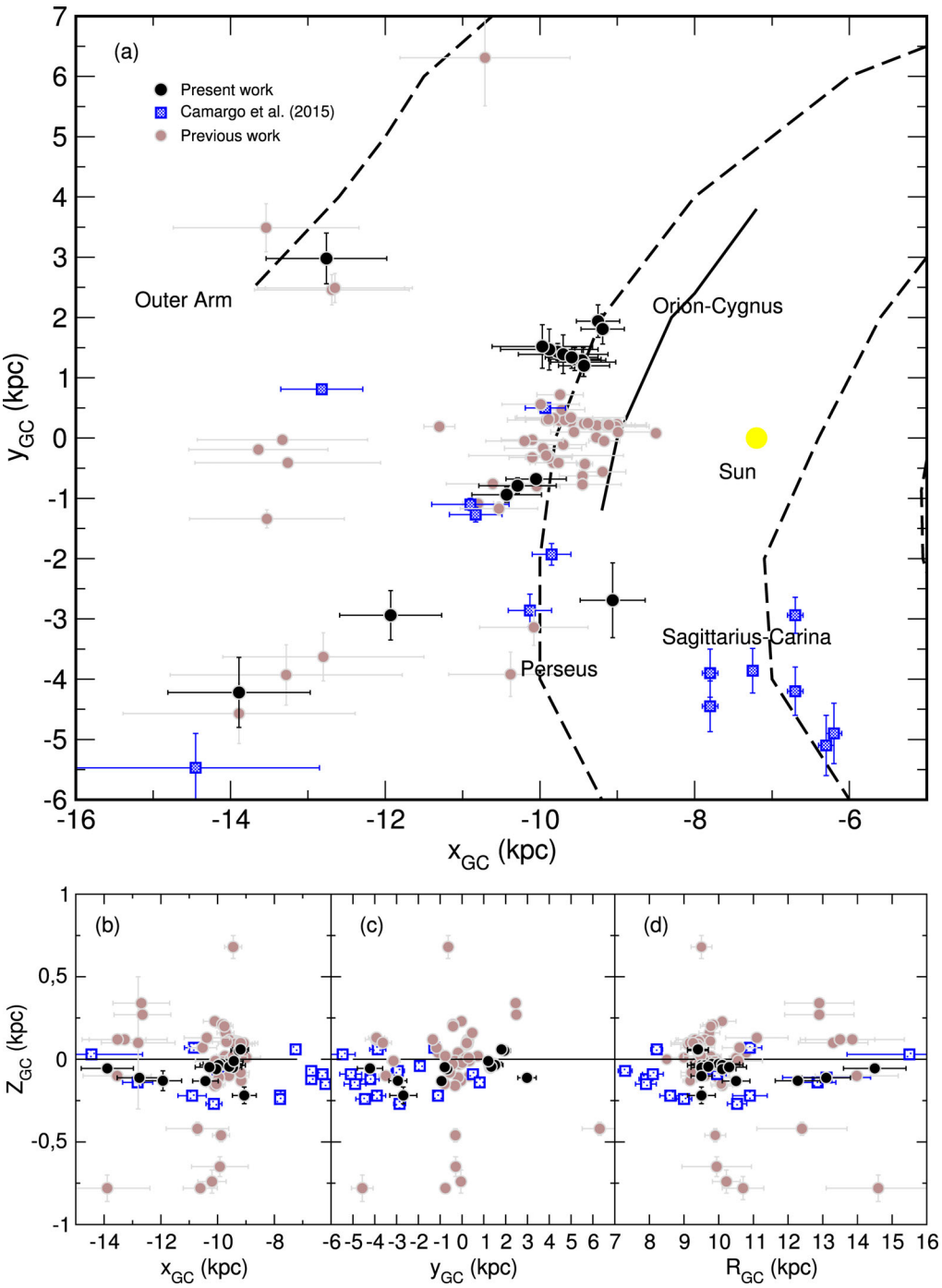

Figure 12. Spatial distribution of the ECs in schematic projection of the Galaxy as seen from the north pole, with 7.2 kpc as the Sun's distance to the Galactic Centre. Black circles are ECs in this work, squares are ECs from Camargo et al. (2015a), and brown circles are ECs in our previous works.

forming a prominent EC aggregate located in the Perseus arm. The present results indicate that in the Galaxy ECs are predominantly located in the spiral arms. Thus, new searches for ECs are important, since they may contribute to the further understanding of the Galaxy structure.

The ECs in the present sample are distributed along three arms, Sagitarius-Carina, Perseus, and Outer arm.

The Sagittarius–Carina spiral arm in the region traced by our EC sample is at a Galactocentric distance of ∼6.4 kpc for $R_\odot = 7.2$ kpc or ∼7.2 kpc for $R_\odot = 8.0$ kpc.

The Perseus arm along the second and third quadrants presents a Galactocentric distance in the range 9–10.5 kpc for a distance of the Sun to the Galactic Centre of 7.2 kpc or in the range of 9.8–11.3 kpc for a $R_\odot = 8.0$ kpc.

The parameters derived for Bochum 2 and C 445 reinforce our previous results for the Outer arm. This feature extends along the second and third Galactic quadrants with a distance from the Galactic Centre in the range of 12.5–14.5 kpc for $R_\odot = 7.2$ kpc or 13.5–15.5 kpc for $R_\odot = 8.0$ kpc.

We find that in the Galaxy most ECs are distributed within the thin disc (∼250 pc) and along spiral arms. However, there occur ECs with $z_{GC} > 500$ pc.

Most massive stars identified in the present EC sample are located within the central region of the cluster ($R < 1$ arcmin).

ACKNOWLEDGEMENTS

We thank an anonymous referee for important comments and suggestions. This publication makes use of data products from the 2MASS, which is a joint project of the University of Massachusetts and the Infrared Processing and Analysis Centre/California Institute of Technology, funded by the National Aeronautics and Space Administration and the National Science Foundation. CB and EB acknowledge support from CNPq (Brazil).

REFERENCES

Allen L. E., Mergeath S. T., Gutermuth R., Myers P. C., Wolk S., Adams F. C., Muzerolle J., Pipher J. L., 2007, in Reipurth B., Jewitt D., Keil K, eds, Protostars and Planets V. Univ. Arizona Press, Tuscan, AZ, p. 361
Anderson L. D., Bania T. M., Balser D. S., Cunningham V., Wenger T. V., Johnstone B. M., Armentrout W. P., 2014, ApJ, 212, 1
Baba J., Asaki Y., Makino J., Miyoshi M., Saitoh T. R., Wada K., 2009, ApJ, 706, 471
Ballesteros-Paredes J., Hartmann L., 2007, Rev. Mex. Astron. Astrofis., 43, 123
Bally J., 2008, in Reipurth B., ed., Handbook of Star Forming Regions, Volume I. Astron. Soc. Pac., San Francisco, p. 459
Bica E., Bonatto C., 2011, A&A, 530, 32
Bica E., Dutra C. M., Barbuy B., 2003a, A&A, 397, 177
Bica E., Dutra C. M., Soares J., Barbuy B., 2003b, A&A, 404, 223
Bica E., Bonatto C., Barbuy B., Ortolani S., 2006, A&A, 450, 105
Bica E., Bonatto C., Camargo D., 2008, MNRAS, 385, 349
Binney J. et al., 2014, MNRAS, 439, 1231
Bobylev V. V., Bajkova A. T., 2014, MNRAS, 437, 1549
Bonatto C., Bica E., 2007a, MNRAS, 377, 1301
Bonatto C., Bica E., 2007b, A&A, 473, 445
Bonatto C., Bica E., 2008, A&A, 485, 81
Bonatto C., Bica E., 2009, MNRAS, 397, 1915
Bonatto C., Bica E., 2010, A&A, 516, 81
Bonatto C., Bica E., 2011a, MNRAS, 414, 3769
Bonatto C., Bica E., 2011b, A&A, 530, 32
Borissova J. et al., 2011, A&A, 532, 131
Bressan A., Marigo P., Girardi L., Salasnich B., Dal Cero C., Rubele S., Nanni A., 2012, MNRAS, 427, 127
Buckner A. S. M., Froebrich D., 2014, MNRAS, 444, 290
Camargo D., Bonatto C., Bica E., 2009, A&A, 508, 211
Camargo D., Bonatto C., Bica E., 2010, A&A, 521, 42
Camargo D., Bonatto C., Bica E., 2011, MNRAS, 416, 1522
Camargo D., Bonatto C., Bica E., 2012, MNRAS, 423, 1940
Camargo D., Bica E., Bonatto C., 2013, MNRAS, 432, 3349
Camargo D., Bica E., Bonatto C., 2015a, New Astron., 34, 84
Camargo D., Bica E., Bonatto C., 2015b, MNRAS, 448, 1930
Carraro G., Vázquez R. A., Moitinho A., Baume G., 2005, ApJ, 630, L153
de la Fuente Marcos R., de la Fuente Marcos C., 2008, ApJ, 672, 342
de la Fuente Marcos R., de la Fuente Marcos C., 2009a, A&A, 500, 13
de la Fuente Marcos R., de la Fuente Marcos C., 2009b, ApJ, 700, 436
de la Fuente Marcos R., de la Fuente Marcos C., 2010, ApJ, 719, 104
Digel S., de Geus E., Thaddeus P., 1994, ApJ, 422, 92
Dobbs C. L., Pringle J. E., 2010, MNRAS, 409, 396
Efremov Y. N., 1995, AJ, 110, 2757
Feigelson E. D. et al., 2011, ApJS, 194, 9
Fellhauer M., Kroupa P., 2005, MNRAS, 359, 223
Francis C., Anderson E., 2012, MNRAS, 422, 1283
Froebrich D., Scholz A., Raftery C. L., 2007, MNRAS, 374, 399
Fujii M. S., Baba J., Saitoh T. R., Makino J., Kokubo E., Wada K., 2011, ApJ, 730, 109
Georgelin Y. M., Georgelin Y. P., 1976, A&A, 49, 57
Glushkova E. V., Koposov S. E., Zolotukhin I. Y., Beletsky Y. V., Vlasov A. D., Leonova S. I., 2010, Astron. Lett., 36, 75
Grand R. J. J., Kawata D., Cropper M., 2012, MNRAS, 421, 1529
Griv E., Lin C.-C., Ngeow C.-C., Jiang I.-G., 2014, New Astron., 29, 9
Guillout P., Sterzik M. F., Schmitt J. H. M. M., Motch C., Neuhaeuser R., 1998, A&A, 337, 113
Hachisuka K., Brunthaler A., Menten K. M., Reid M. J., Hagiwara Y., Mochizuki N., 2009, ApJ, 696, 1981
Heyer M. H., Terebey S., 1998, ApJ, 502, 265
Honma M. et al., 2007, PASJ, 59, 889
Hou L. G., Han J. L., 2014, A&A, 569, A125
Hou L. G., Han J. L., Shi W. B., 2009, A&A, 499, 473
Jose J. et al., 2013, MNRAS 432, 3445
Kaltcheva N. T., Hilditch R. W., 2000, MNRAS, 312, 753
King I., 1962, AJ, 67, 471
Kumar M. S. N., Kamath U. S., Davis C. J., 2004, MNRAS, 353, 1025
Lada C. J., Lada E. A., 2003, ARA&A, 41, 57
Lee E. J., Murray N., Rahman M., 2012, ApJ, 752, 146
Lennon D. J., Dufton P. L., Fitzsimmons A., Gehren T., Nissen P. E., 1990, A&A, 240, 349
Lépine J. R. D., Roman-Lopes A., Abraham Z., Junqueira T. C., Mishurov Y. N., 2011, MNRAS, 414, 1607
Levine E. S., Blitz L., Heiles C., 2006, Science, 312, 1773
Lima E. F., Bica E., Bonatto C., Saito R. K., 2014, A&A, 568, 16
McClure-Griffiths N. M., Dickey J. M., Gaensler B. M., Green A. J., 2004, ApJ, 607, 127
Majaess D., 2013, Ap&SS, 344, 175
Majaess D. J., Turner D. G., Lane D. J., 2009, MNRAS, 398, 263
Martínez-García E. E., González-López lira R. A., 2013, ApJ, 765, 105
Mercer E. P. et al., 2005, ApJ, 635, 560
Moffat A. F. J., Vogt N., 1975, A&AS, 20, 85
Moffat A. F. J., Jackson P. D., Fitzgerald M. P., 1979, A&AS, 38, 197
Munari U., Carraro G., 1995, MNRAS, 277, 1269
Pandey A. K., Sharma S., Ogura K., 2006, MNRAS, 373, 255
Pettitt A. R., Dobbs C. L., Acreman D. M., Price D. J., 2014, MNRAS, 444, 919
Roca-Fàbrega S., Valenzuela O., Figueras F., Romero-Gómez M., Velázquez H., Antoja T., Pichardo B., 2013, MNRAS, 432, 2878R
Roman-Duval J., Jackson J. M., Heyer M., Johnson A., Rathborne J., Shah R., Simon R., 2009, ApJ, 699, 1153
Russeil D., 2003, A&A, 397, 133
Russeil D., Adami C., Georgelin Y. M., 2007, A&A, 470, 161
Santos-Silva T., Gregorio-Hetem J., 2012, A&A, 547, 107

Sellwood J. A., 2010, MNRAS, 409, 145
Sellwood J. A., 2011, MNRAS, 410, 1637
Sellwood J. A., Carlberg R. G., 2014, ApJ, 785, 137
Siebert A., Bienaymé O., Soubiran C., 2003, A&A, 399, 531
Siebert A. et al., 2012, MNRAS, 425, 235
Skrutskie M. F. et al., 2006, AJ, 131, 1163
Solin O., Haikala L., Ukkonen E., 2014, A&A, 562, 115
Stephenson C. B., Sanduleak N., 1971, Publ. Warner Swasey Obs., 1, 1
Tamburro D., Rix H.-W., Walter F., Brinks E., de Blok W. J. G., Kennicutt R. C., Mac Low M.-M., 2009, AJ, 136, 2872
Turbide L., Moffat A. F. J., 1993, AJ, 105, 1831
Vallée J. P., 2005, AJ, 130, 569
Vallée J. P., 2014a, AJ, 148, 5
Vallée J. P., 2014b, MNRAS, 442, 2993
Vallenari A., Bertelli G., Schmidtobreick L., 2000, A&A, 361, 73
Vogt N., Moffat A. F. J., 1972, A&AS, 7, 133

This paper has been typeset from a TEX/LATEX file prepared by the author.